AEROTHERMAL MODELING PROGRAM - PHASE II*

H.C. Mongia, S.V. Patankar[†], S.N.B. Murthy,[‡] J.P. Sullivan,[‡]
and G.S. Samuelsen[§]

Allison Gas Turbine Division, General Motors Corporation

The main objectives of the NASA-sponsored Aerothermal Modeling Program, Phase II
are:

o to develop an improved numerical scheme for incorporation in a 3-D combustor
   flow model
o to conduct a benchmark quality experiment to study interaction of primary jet
   with a confined swirling crossflow and to assess current and advanced turbu-
   lence and scalar transport models
o to conduct experimental evaluation of the air swirler interaction with fuel
   injector, assessment of the current two-phase models, and verification of the
   improved spray evaporation/dispersion models

To improve predictive capabilities of current combustor aerothermal models, im-
provements are needed in numerical schemes, modeling of turbulence and scalar
transport processes, and spray modeling of interaction with turbulent recirculating
swirling flows. To assess current models and help the development of advanced
models, detailed and accurate experimental data are needed for well defined test
configurations. The main objective of the NASA Aerothermal Program is to provide
the gas turbine combustion community with benchmark quality data and significantly
improved numerical scheme, turbulence, scalar, and spray transport models.

There are three elements of the Aerothermal Modeling program--Phase II. They are:

Element A - Improved Numerical Methods for Turbulent Viscous Recirculating Flows
Element B - Flow Interaction Experiment
Element C - Fuel injector - Air Swirl Characterization
Each element will be briefly described.

I.   IMPROVED NUMERICAL METHODS FOR TURBULENT VISCOUS RECIRCULATING FLOWS

The advanced numerics effort consists of the following three technical tasks. Task
1 has been completed and Task 2 is under progress.

Task 1.   Numerical Methods Selection

The first phase of Task 1 involved the selection of at least six numerical tech-
niques. These techniques were evaluated in the second phase of Task 1. Based on
this preliminary evaluation four techniques were chosen for detailed evaluation
under Task 2. The selected schemes had to be more accurate than the conventional
upwind differencing (UD) and hybrid schemes; in particular the numerical schemes
had to minimize the numerical diffusion encountered in UD and hybrid schemes for
grid Peclet numbers greater than two. In addition, the schemes had to be stable,
bounded, and computationally efficient for a wide range of Peclet numbers and a
broad class of problems.

[†]University of Minnesota
[‡]Purdue University
[§]University of California at Irvine

Among the techniques chosen for preliminary evaluation were the finite element scheme of Baliga and Patankar, the cubic-spline method, the skew upwind differencing scheme (SUDS), the quadratic upwind differencing scheme (QUDS or QUICK), the flux-blended versions of SUDS and QUDS, the Agarwal fourth order scheme, the exponential (tabulated) scheme, and Patankar's flux-spline schemes. As a first step an extensive literature survey was conducted, firstly, to derive conclusions regarding the relative merits of the various schemes based on comparative studies reported in the literature and secondly, to identify new schemes or techniques to modify existing schemes. The survey showed that while many of the schemes are considerably more accurate than the hybrid scheme for specific test cases, no second order scheme is currently available that is unconditionally stable, bounded, and conservative. Therefore, an effort was initiated to focus on modifying an existing scheme and/or developing a new scheme that would meet the objectives of the program. In addition, the task of identifying the most promising techniques among those listed continued with the application of the various techniques to test problems. The result of these two efforts are summarized in the following paragraphs.

A number of test problems were chosen and solved by different numerical schemes. Of all the schemes studied the flux-spline scheme (and its variants) and the quadratic upwind scheme (QUICK) seemed to perform significantly better than the other schemes. The basic flux-spline scheme assumes that the total flux J (convection + diffusion) of the dependent scalar variable ϕ, varies linearly with distance over each control volume. Two versions of the scheme result from the assumption of a stepwise and piecewise linear velocity distribution, respectively, for the underlying convection field. The improved flux-spline scheme is based on a cubic variation of the total flux J as well as the underlying velocity. The QUICK (or QUDS) scheme seemed to show the best performance among the schemes studied under the NASA Error Reduction Program at Pratt and Whitney, (see reference 1) although the stability and means of improving the solution technique for the scheme were vastly unexplored. In particular, the flux-blending scheme, to keep the solution bounded, was not incorporated in the QUDS scheme for various reasons. Therefore, the bounded QUICK scheme is considered to merit further exploration in the present study.

Efforts to develop a new second order scheme resulted in the controlled numerical diffusion with internal feedback (CONDIF) scheme (developed by Runchal), which is a modified central differencing scheme (CDS). CONDIF recasts the centered-difference equation in a form that leads to unconditional stability and low numerical diffusion. Results for sample test problems show improved accuracy over those for the hybrid scheme, especially at high Peclet numbers. CONDIF retains the second order accuracy of CDS, but unlike CDS is unconditionally stable and devoid of over and under-shoots in the solution of the dependent variable.

Another aspect of Task 1 concerns the selection of a suitable solution algorithm for the flow field. The momentum and continuity equations represent a nonlinear coupled set that must be solved to get a prediction for the flow field. Iterative methods such as SIMPLE and SIMPLER have been developed to solve the flow equations. These methods, although quite successful, have proved to be slowly converging and hence time consuming. Their success also depends on the proper choice of under-relaxation factors. An alternative to these iterative methods is the direct solution of the whole set of momentum and continuity equations. This alternate method uses the D'Yakonov iteration scheme and the Yale University Sparce Matrix Package. Preliminary investigation of two schemes based on the direct solution method showed that the schemes converged considerably faster than SIMPLE AND SIMPLER.

90

Based on the findings under Task 1, the following four techniques were selected for further evaluation Task 2:

1. Flux-spline scheme and its variants
2. CONDIF scheme
3. Bounded QUICK scheme
4. Direct solution methods

Task 2--Technique Evaluation

Under Task 2, the techniques selected in Task 1 will be tested extensively in terms of accuracy, stability, and computational efficiency. The techniques will be used to calculate a variety of test cases including 2-D recirculating flows-turbulent and non-turbulent, with and without swirl. The first step, which is currently under progress, is to identify the test cases for which accurate numerical or analytical solutions or detailed experimental data exist. The techniques will be used to calculate the selected test cases and the technique showing the best performance will be incorporated in Task 3.

Task 3--3-D Computation Evaluation

An existing NASA Lewis 3-D elliptic code (COM3D) will be modified to incorporate the "best" advanced numerical scheme identified in Task 2. A test case will be selected including the geometry, experimental data, and computational details. This case will be run to assess the performance of the advanced numerical scheme including accuracy, stability, convergence rate, and computational time.

II. FLOW INTERACTION EXPERIMENT

This element consists of both experimental and numerical investigations that include five major technical tasks as discussed in the following:

Task 1--Experimental Configuration

This task involved preliminary design of the test section, its detailed design for fabrication and the experimental plan for data acquisition. A layout for the test section geometry is shown in Figure 1 with photographs shown in Figure 2. The 30-in. long test section made of plexiglass to facilitate optical access for the LDV has rectangular cross-section (15 in. x 3 in.) The main flow is established using five swirlers and the primary jets are injected in cross-flow as shown in the figure. Under this task, two similar rigs - one using air for LDV measurements and the other using water for flow visualization have been designed.

The detailed test matrix for the Flow Interaction program is given in Figure 3 and the corresponding flow configurations are shown in Figure 4. The configuration changes are made in both the air and water rigs with interchangeable upper and lower plates.

The first two tests have no fluid entering through the primary jets. Test 1 admits nonswirling fluid through five annular jets while Test 2 uses 60 deg flat vane swirlers. Tests 3 through 6 involve the interaction of swirling flow with the flow from two primary jets. The mass flow ratio and the downstream distance is the same for these cases with the cross-channel location and the stagger of the jets varying as shown in Figures 4A through 4D. The effect of downstream location of the two primary jets is investigated in Tests 9 and 10 and the effect of mass flow ratio

in Tests 14 and 15. A similar set of experiments involving four primary jets per swirler is scheduled in Tests 7, 8, 11, 12, 16 and 17. The four jet configurations are shown in Figures 4E and 4F.

Task 2--Modeling

This task involved the selection of a 3-D flow code and simulation of different flow configurations using the current turbulence model ($\kappa-\varepsilon$) for a preliminary study of the flow fields. The main importance of the task has been in highlighting different vortical regions in the flow field that would be taken into account during LDV measurements so as to resolve these regions of steep velocity gradients. For the purpose of numerical simulation, the COM3D computer code was selected. Each flow configuration was computed using a 35 x 25 x 25 grid that was uniform in the y-z plane and nonuniform along the x-direction (the main flow direction). The solution convergence was typically obtained in about 200 iterations.

The results of computing the chosen basic flow configurations (See Figure 4) indicate that these configurations indeed offer interesting flow fields for the final verification/validation of the model against the data base. For example, some results for configuration B are shown in Figures 5 and 6. A complex interaction between the swirling flow and the jets in cross-flow is clearly seen. For $Xj/H = 0.5$, Figure 5C shows two concentrated vortices, one at the upper right-hand corner and the other at the lower left-hand corner. In these regions the primary jets are aiding the angular momentum of the swirling flow. With the reduced swirl downstream at $Xj/H = 1.0$, the interaction with the jets results in larger vortical regions in the cross-plane as shown in Figure 6.

Task 3--Measurements

Two test rigs and various test configurations have been fabricated under Task 3. The test rigs along with the associated instrumentation have been assembled and initial checkout runs have been made to ensure that the rig, instrumentation, and data reduction software are performing well.

The flow visualization rig will be used to establish flow characteristics and define regions of interest for conducting detailed single-point measurements.

For the flow configurations identified in Task 1, measurements will be made to obtain the following:

o detailed wall static pressure distribution
o mean velocity and Reynolds stress components
o fluctuating and mean concentration measurements for assessing scalar transport models

Velocity measurements are made with a two-color, two-component LDV system, shown in Figure 7, is mounted on a computer-controlled table that along with computer control of the field lens allows movement of the probe volume in three dimensions.

The data acquisition system consists of TSI counter type processors interfaced to a DEC 11/23 computer (See Figure 8). The hardware interface contains a resetable 10 MHZ clock for measuring the time of arrival of a valid LDV signal. The simultaneous arrival of signals from the two components is determined in software by requiring that the respective clock signals are within 1-microsecond of each other.

The DEC 11/23 also controls the x-y-z position of the probe volume through a stepper motor controller.

The three beam optical arrangement allows measurements to be made close to a wall. By rotating the optics package about the optical axis, measurements near the end-wall, top wall, and bottom wall are possible.

Detailed velocity measurements are underway and the results will be presented during the meeting.

Task 4--Results and Analysis

Under this task, measurements of velocity and smoke concentration will be analyzed to determine the probability density function and auto- and cross-correlations.

Task 5--Model Improvement

This task involves the development and use of improved turbulence and scalar transport models for complex swirling flows.

III.   FUEL INJECTOR--AIR SWIRL CHARACTERIZATION

This element, which covers both experimental and numerical research on two-phase flow interactions to support analytical modeling of the dome region of the combustor, consists of five major tasks. Tasks 1 and 2 have been completed. A brief description of the five tasks is given in the following paragraphs.

Task 1--Experimental Configuration

This task involves preliminary design of the test section, its detailed design for fabrication, and the experimental plan for data acquisition.

The proposed experiment will consist of a fuel injector and a swirler typical of current use in aircraft turbine engines (See Figure 9). The fuel nozzle and swirler combination will be run at both free of confinement and confined conditions (6-in. duct). The experimental plan will cover a wide range of tests that could be staged in complexity, with the constituent flows measured separately and then in combination. The duct is designed in such a way to enable the required measurements to be taken at the inlet plane and at seven axial locations downstream of the swirler-fuel injector combination. The measurements will include the following quantities: the three components of mean and root mean square (rms) gas velocity as well as Reynolds stresses, the three components of mean and rms droplet velocity, Sauter mean diameter, droplet size distribution, spatial distribution of droplets, cone angle, fraction of liquid evaporated in the duct (vapor concentration), the static pressure along the wall of the duct, and the inlet air temperature.

All the test configurations (See Figure 10) will first be operated free of injected particles (expert for the Laser anemometer seed), second with injected monodisperse solid particles (30-micron glass beads), then with injected multi-sized solid particles (30, 50, and 100 µm glass beads), and finally with a fuel spray (methanol).

Task 2--Modeling Sensitivity Analysis

Allison had run its 2-D codes (parabolic and elliptic) to predict the distribution of the flow field variables for all proposed flow and geometry test conditions of the experimental test matrix. The main purpose of this task is to determine if the planned experiment is sensitive to the significant variables and which variables and boundary conditions are necessary to measure.

As proposed in Allison EDR 11754, the COMDISP code (the modified version of the OCG-2 computer code of Brigham Young group) has been run to predict the test plan cases. Two cases will be demonstrated. The first case represents single-phase flow (no injected particles) through the primary tube and air swirler of 60 deg in a 6-in. duct. Figure 11 shows that the main flow is attached to the wall (first radially outward then axially forward). This finding is in complete agreement with the simple flow visualization studies done at Purdue University under Element B of the HOST program. To get a good flow pattern in the duct, it has been suggested that the swirler be recessed into the head plate by 1/4-in. for the test matrices of both Elements B and C of the HOST program.

The second case represents a fuel nozzle centered in 1.5-ft duct to simulate a free of confinement conditions thus allowing the spray to be characterized in the absence of wall effects. A low stream of air through the duct will be used to suppress recirculation and the subsequent accumulation of aerosol. Even with this low stream (.5 m/s) a weak recirculation bubble has been formed near the wall but farther downstream from the exit plane (See Figure 12). In this case, the problem can not be predicted using a parabolic code that does not consider the wall effects. This turns down the main function of the big duct. Accordingly, Allison has suggested to replace the 1.5-ft plexiglass duct by a screen enclosure. The screen will allow the necessary air, demanded by the jet entrainment, to enter the chamber and thereby preclude wall recirculations.

Task 3--Measurements

The efforts of the first year have been directed to (1) the design, fabrication, and testing of the facility, (2) the preliminary verification of the laser interferometer diagnostics (See Figure 13), and (3) the acquisition of test data in the spray chamber.

In the present program, the utility, applicability, and accuracy of phase Doppler has been tested in a series of experiments in which pitch diameter (PD) has been compared to visibility/intensity validation and laser diffraction using a Malvern, (See References 2 and 3). Basically, two comparisons are considered: radial variation in SMD and composite weight distributions, both at selected axial locations in a air assist nozzle operating on water as the liquid.

The radial variation of the spatial SMD of the spray is depicted in Figure 14 for axial positions of 30-mm and 50-mm. In each case, the single line-of-sight Malvern measurement (from both the Rosin Rammler and Model Independent Analyses) is also illustrated. The correspondence between the two interferometric measurements is very good at both axial stations. Differences that surface are realistic in light of the relative limitations of the instruments. The phase Doppler was configured to measure diameters as small as 1-micron, whereas the V/IV was configured to measure diameters as small as 6-microns. The large sizes typical of the outer regions of the spray, require a change in the V/IV optics and concomitant splicing of data. For example, at 30-mm the outer two data points are each composites of two separate

94

measurements; at 50-mm the outer three points are composites of eight data runs, splicing different size windows and frequency bands. In addition to being somewhat tedious, the required splicing of data sets introduces potential error in that the method of splicing data points is uncertain. Note that, at 50-mm, there is a shift in the data as the spliced sets are encountered.

Comparing the point measurements to the single line of sight measurement is encouraging. Both interference techniques give plausible radial profiles of SMD in light of the diffraction measurement.

At 30-mm PD yields a composite SMD of 31.8-microns (weighted in addition by the radial growth of the effective probe volume); V/IV measures 28.9-microns. The Malvern yields values of 19.5-microns (Rosin Rammler) and 28.3-microns (Model Independent). At 50-mm the PD composite value of 29.4-microns; that of V/IV is 31.9-microns. The Malvern yields values of 24.4-microns (Rosin Rammler) and 30.7-microns (Model Independent). At both locations the correspondence between point measurements and the Model Independent analyses of diffraction data is excellent. The Rosin Rammler value is typically low, suggesting it does not adequately fit the diffraction data.

In Figure 15, the same data sets are examined in terms of their distribution of liquid weight. Distributions from the point measurements are composites, generated in a manner consistent with the composite SMD formulation. The Rosin-Rammler distributions are plotted on the same scale as the Model Independent distributions (15 parameter curve fit) for the same data. The size intervals represented by each point vary in accordance with the size and radial position of elements of the focal plane detector. Although both the Rosin-Rammler and Model Independent distributions compare favorably at this axial location, the point measurements agree better with the Model Independent treatment of the diffraction data in locating the distribution's peak. The apparent divergence of the diffraction data at large drop sizes is an artifact of plotting the data in the size intervals of the Model Independent algorithm (the resolution of the distribution model decreases in inverse proportion to drop size).

Task 4--Results and Analysis

Experimental data of Task 3 will be reduced and presented in a format suitable to make direct comparison with model predictions and to quantify the effects of the flow and geometric variables in various transport processes.

Task 5--Model Improvement

An advanced spray/flow interaction model will be validated under this effort. The model will include improved submodels of turbulence, spray injection, trajectory, evaporation, particle dispersion, and scalar transport processes.

REFERENCES

1. Syed, S.A., Chiapetta, L.M., and Gosman, A.D., Error Reduction Program, Final Report, NASA CR-174776, January 1985.

2. Jackson, T.A., and Samuelsen, G.S. "Spatially Resolved Droplet Size Measurements," ASME 85-GT-038, ASME Gas Turbine Conference, Houston, TX (Accepted for publication in Journal of Engineering for Gas Turbines and Power). 1985.

3. Jackson, T.A., and Samuelsen, G.S. "Performance Comparison of Two Interferometric Droplet Sizing Techniques," SPIE 573-09, Society of Photo-Optical Instrumentation Engineers 29the Annual International Technical Symposium, San Diego, CA. 1985.
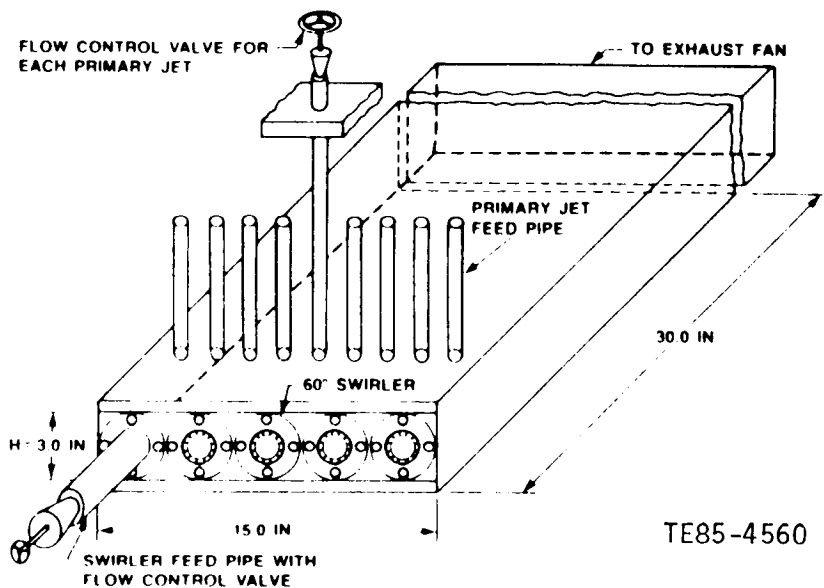
Figure 1.   Test section geometry.
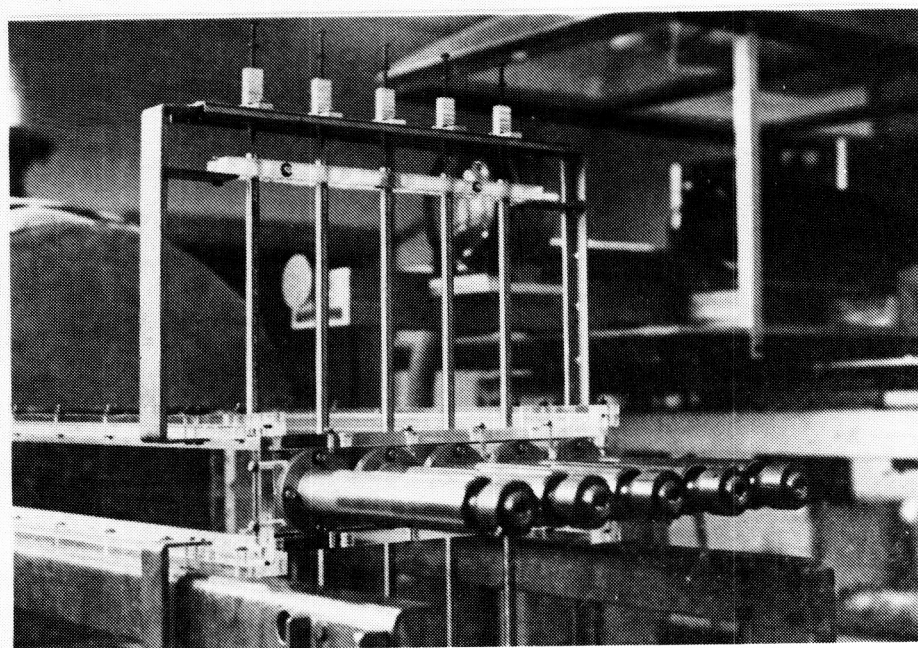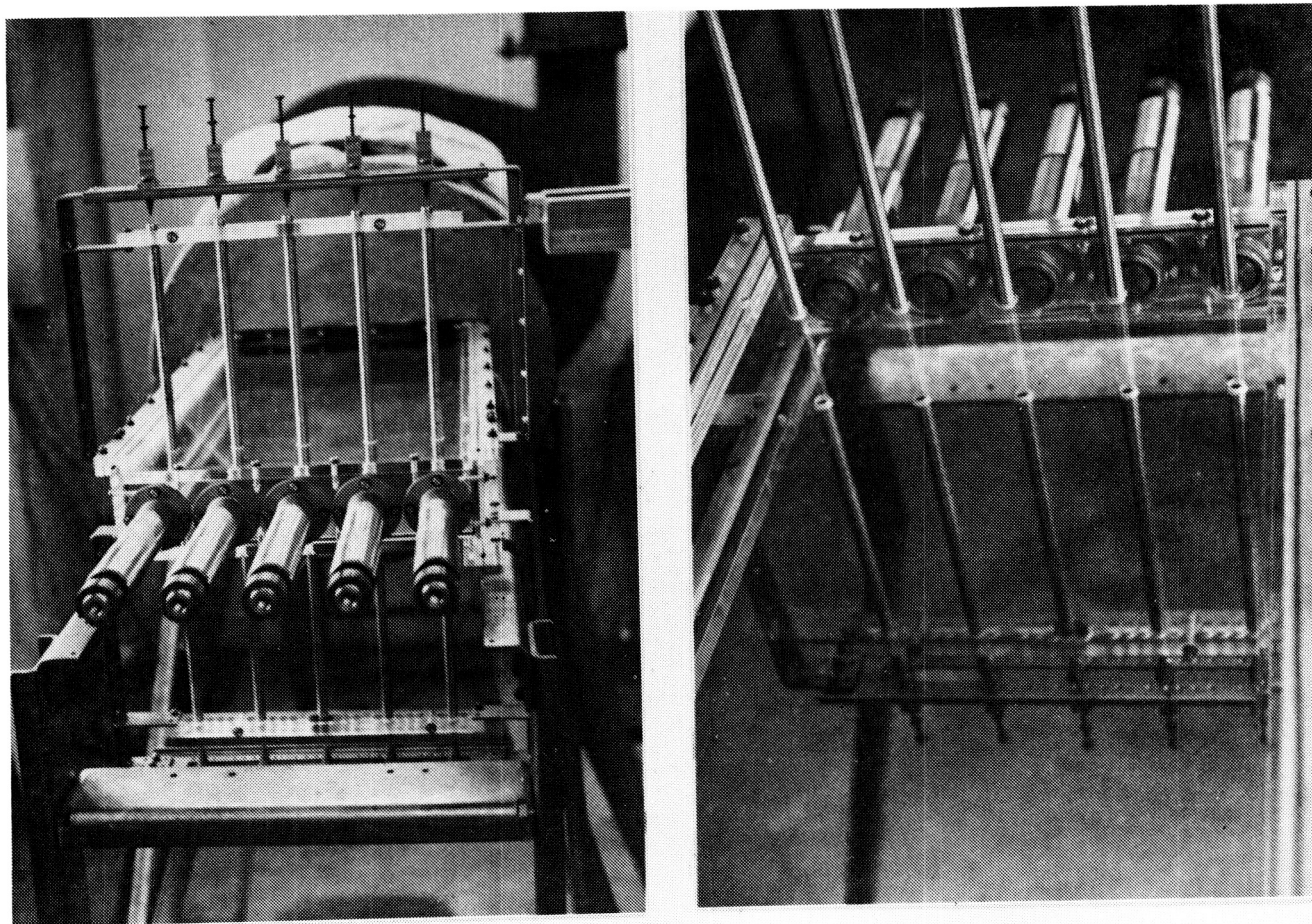
TE85-4561

Figure 2.   Flow interaction experiment – air rig.

Test No.	Configuration	ξ_j/H	X_j/H	M_j/Ms	Tracer	Jets/swirler
1	BC1	–	–	–	No	–
2	BC2	–	–	–	No	–
3	A	1.0	0.5	0.75	No	2
4	B	1.0	0.5	0.75	No	2
5	C	1.0	0.5	0.75	No	2
6	D	1.0	0.5	0.75	No	2
7	E	0.5	0.5	1.50	No	4
8	F	0.5	0.5	1.50	No	4
9	A	1.0	1.0	0.75	No	2
10	B	1.0	1.0	0.75	No	2
11	E	0.5	1.0	1.50	No	4
12	F	0.5	1.0	1.50	No	4
13	A	1.0	0.5	1.50	No	2
14	A	1.0	0.5	0.75	Yes	2
15	B	1.0	0.5	0.75	Yes	2
16	E	0.5	0.5	1.50	Yes	4
17	F	0.5	0.5	1.50	Yes	4
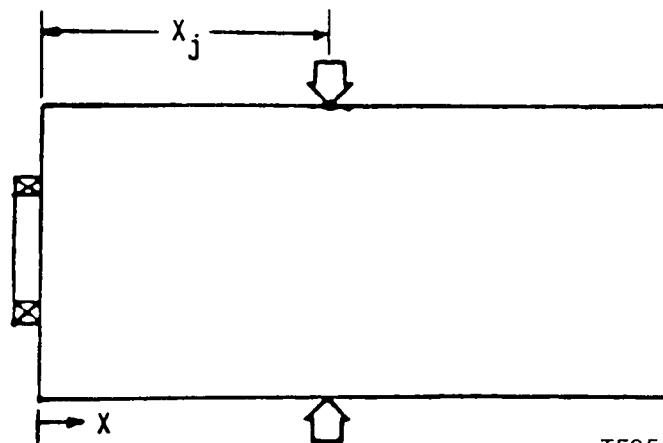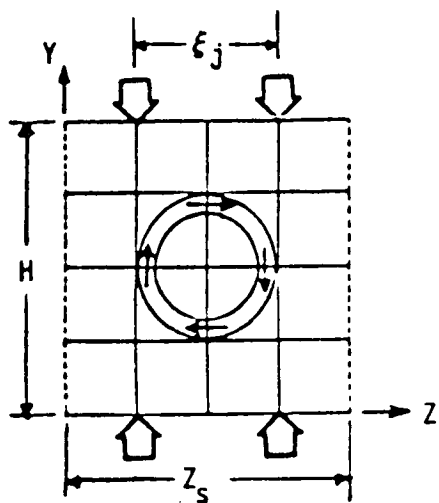
TE85-4567

Figure 3.   Text matrix.
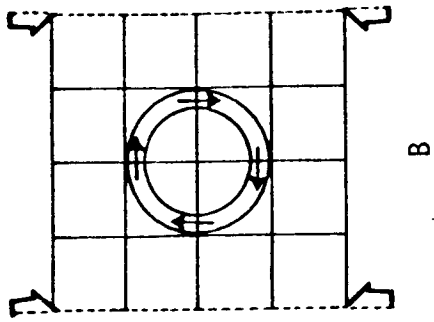
Baseline Case 1
(BC1)
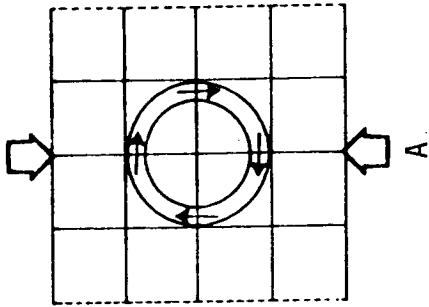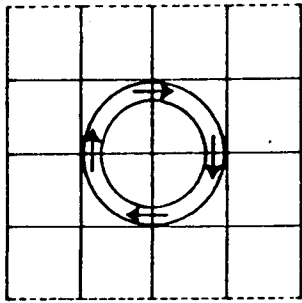
Baseline Case 2
(BC2)

A

B

C

D

E

F
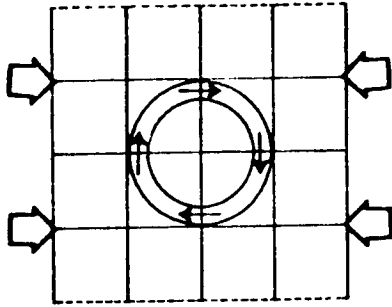
TE85-1821
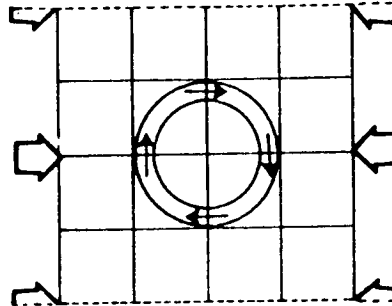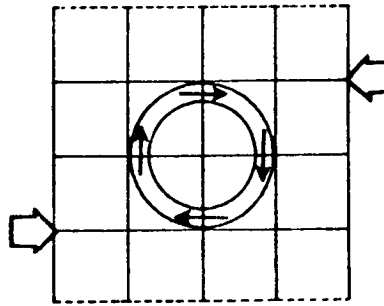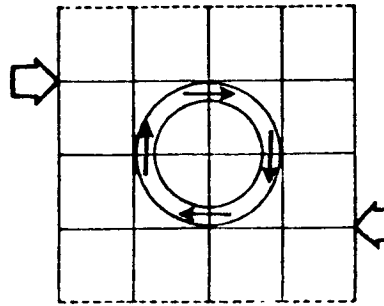
Figure 4.   Basic flow configuration.

99
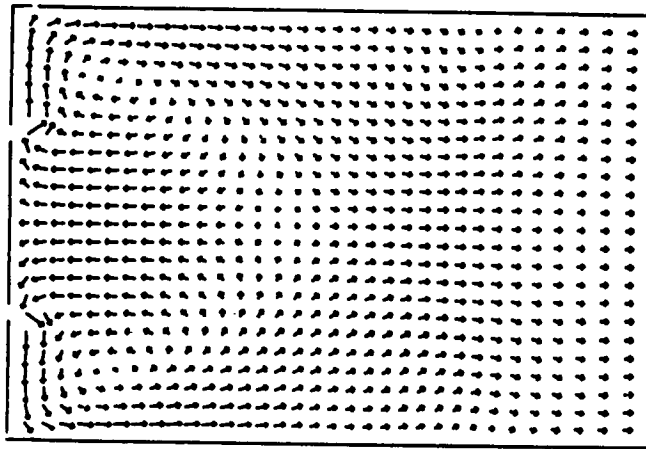
a. Midswirler plane (X-Y)
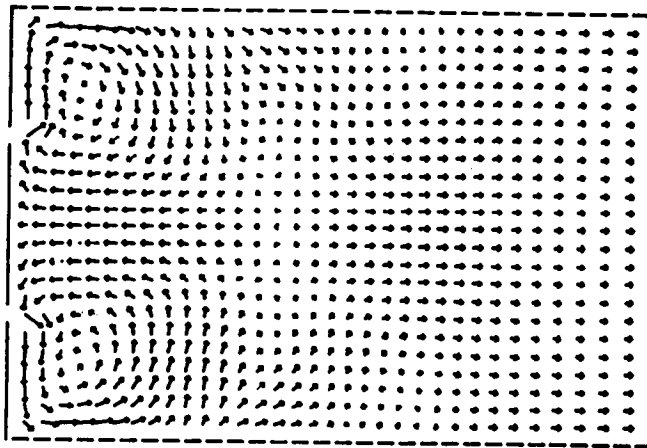
b. Midswirler plane (X-Z)
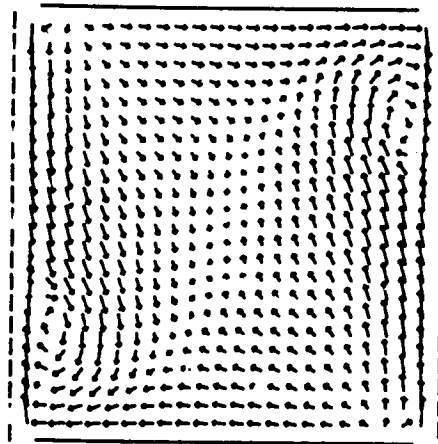
c. Transverse plane (Y-Z) through jet axes

TE85-1983

Figure 5.   Velocity fields for configuration B; Xj/H=0.5.
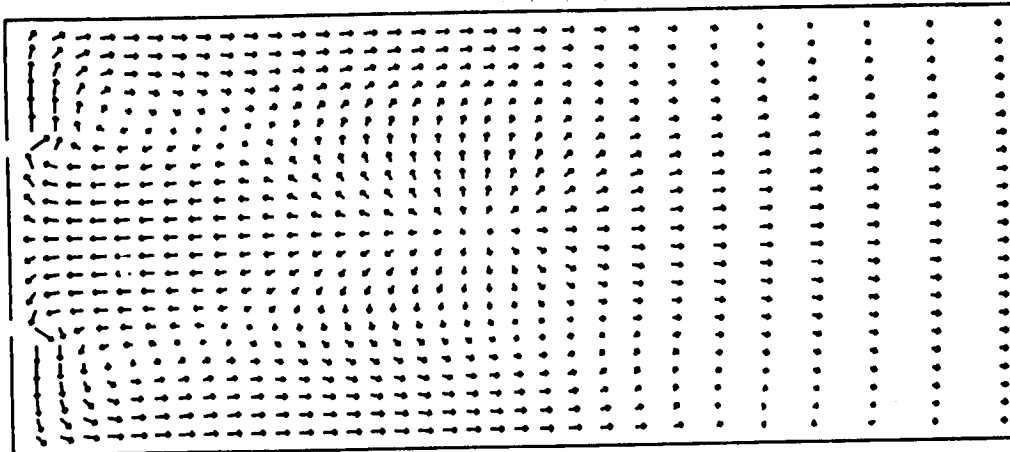
a. Midswirler plane (X-Y)
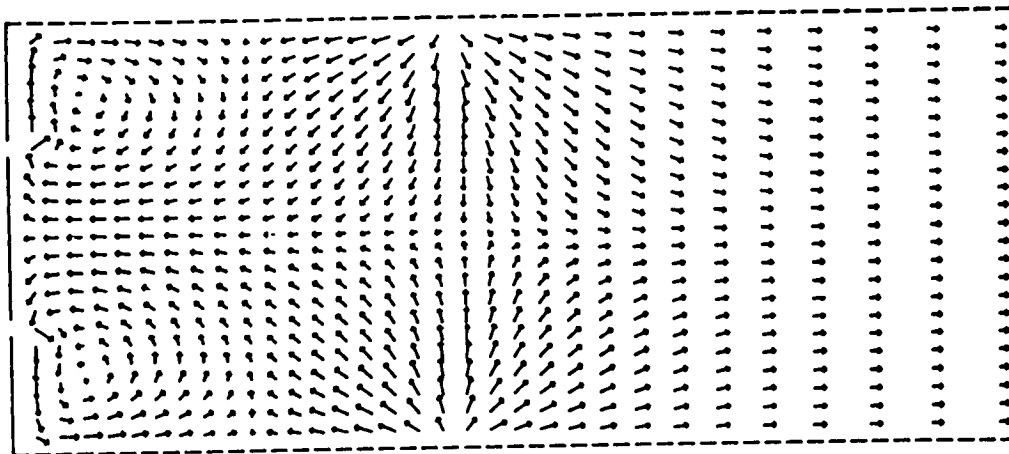
b. Midswirler plane (X-Z)
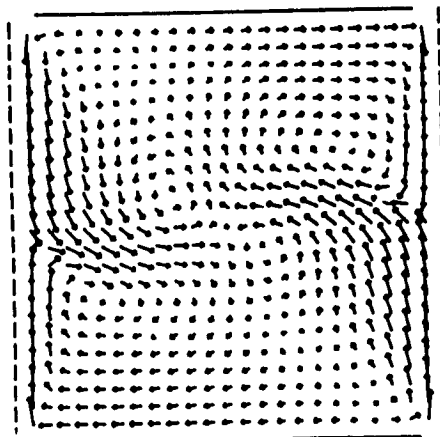
c. Transverse plane (Y-Z) through jet axes

TE85-1984

Figure 6.   Velocity fields for configuration B; Xj/H-1.0.
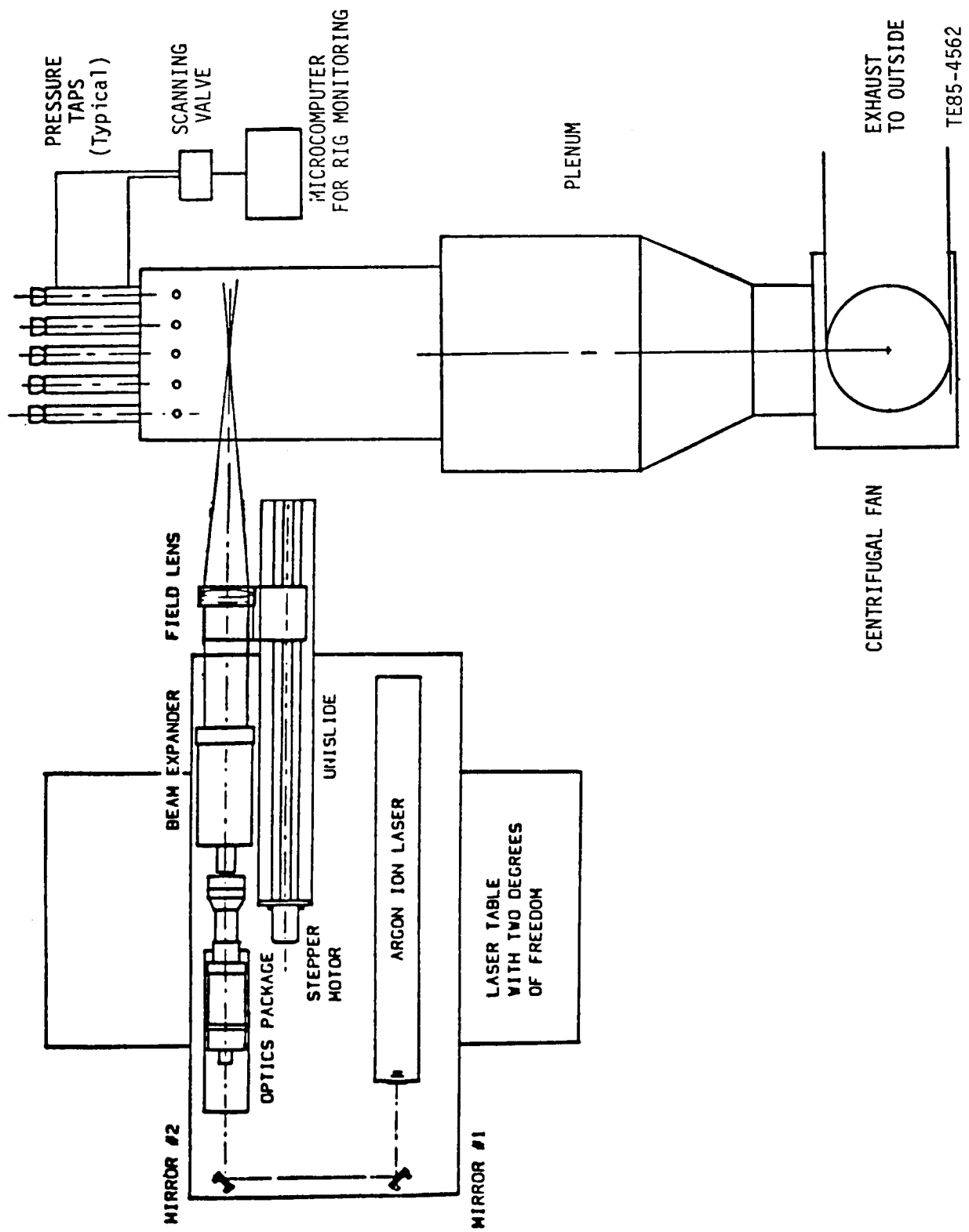
Figure 7.   LDV system for flow interaction experiment.
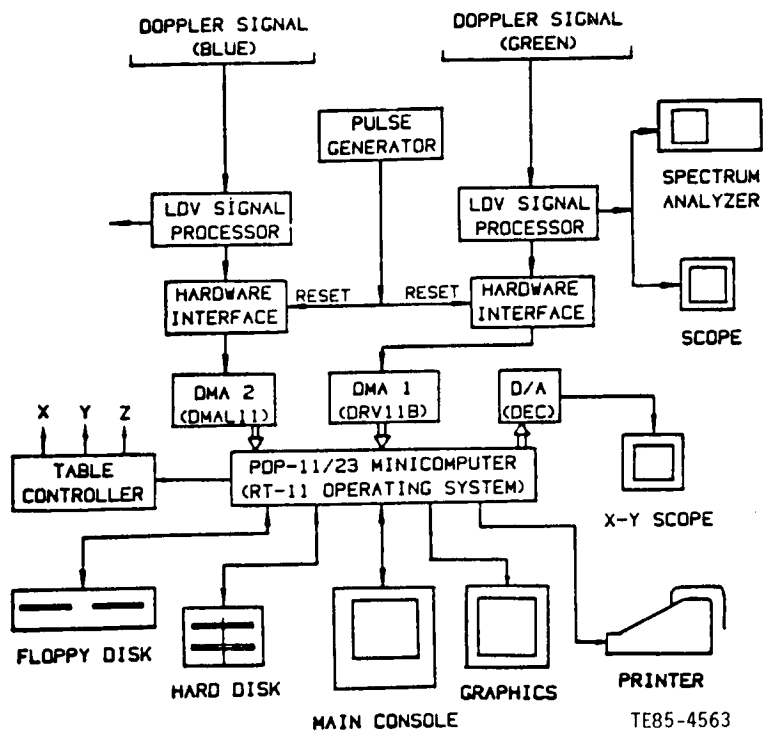
Figure 8.   Data acquisition system for LDV.
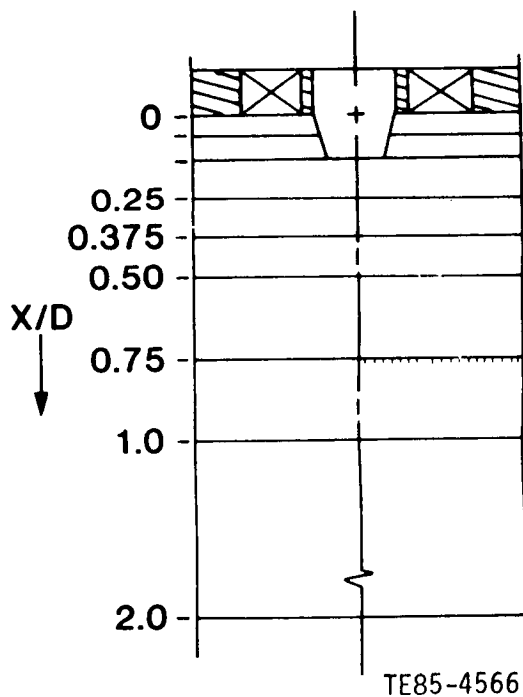
Figure 9.   Experimental configuration for confined flow with
                liquid fuel injection and swirl.9
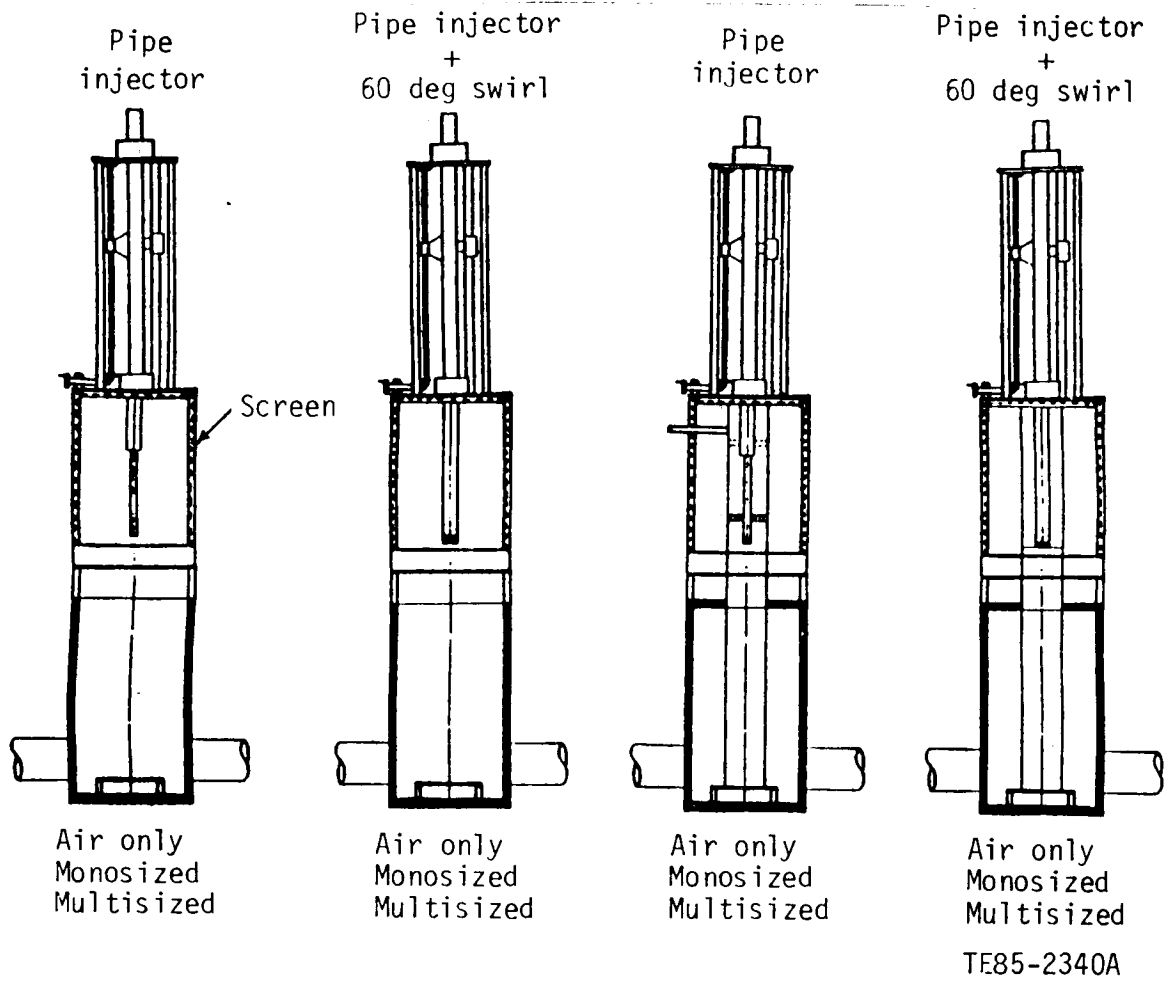
Figure 10.   Experimental configurations.
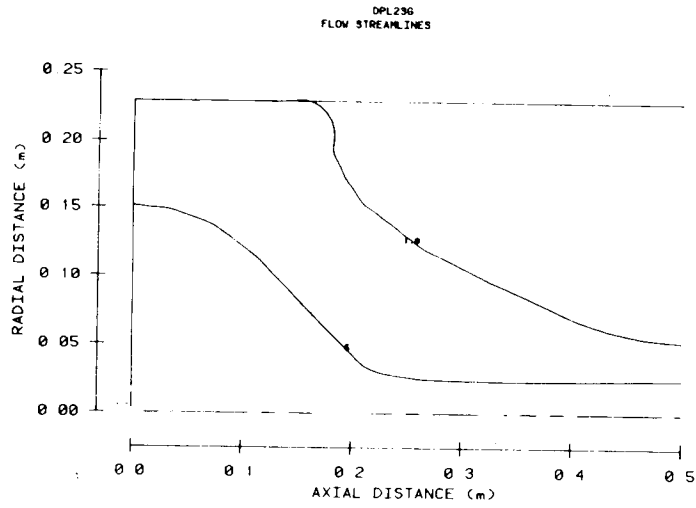
GASPLT6
FLOW STREAMLINES
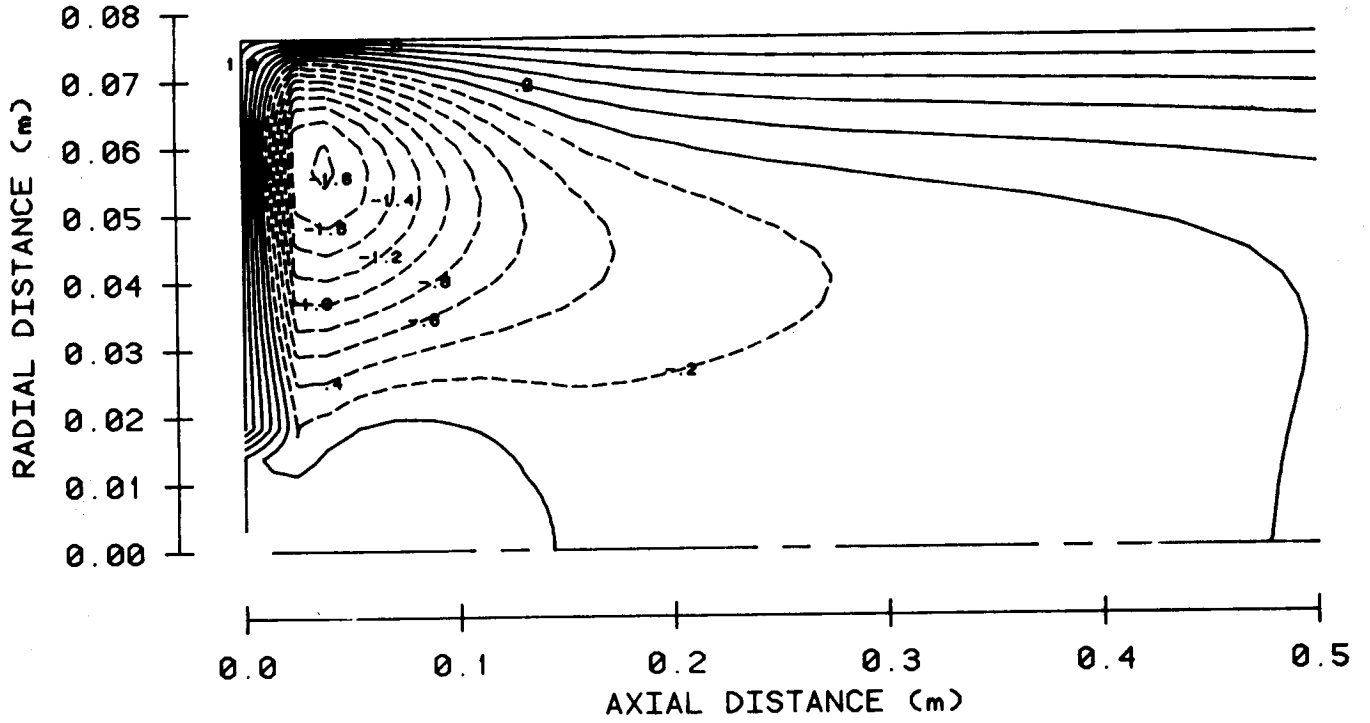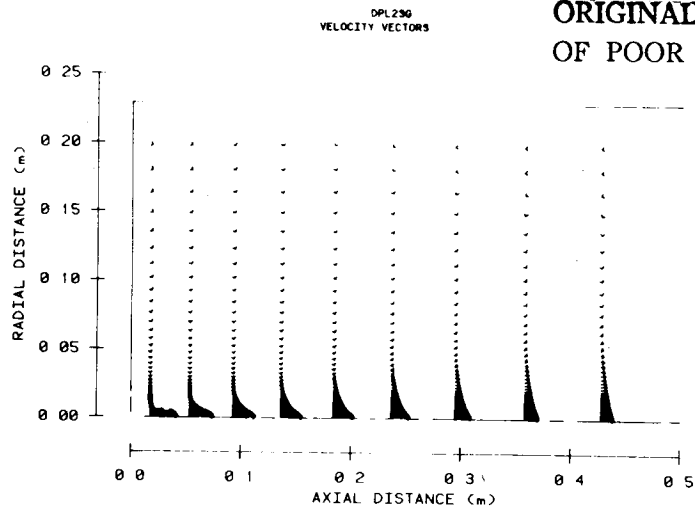

GASPLT6
VELOCITY VECTORS
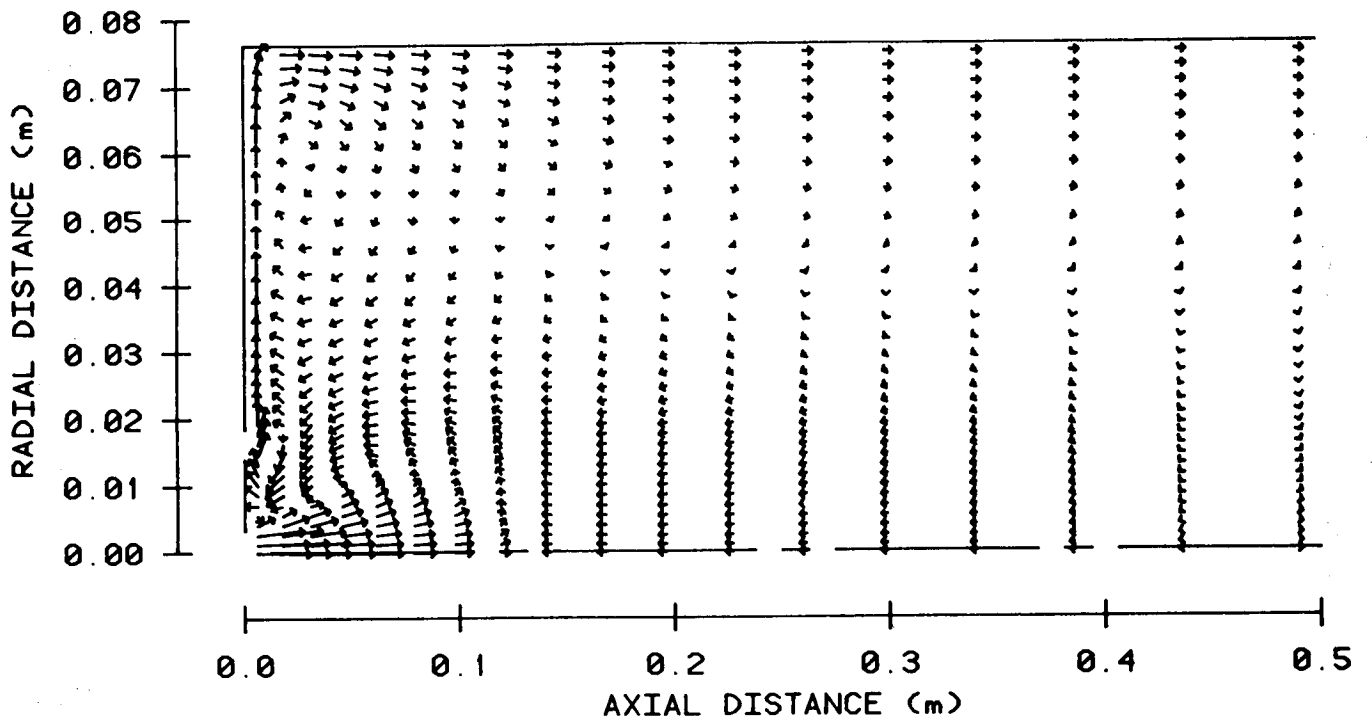
TE85-2346

Figure 11.   Air only cases at confined conditions (particles
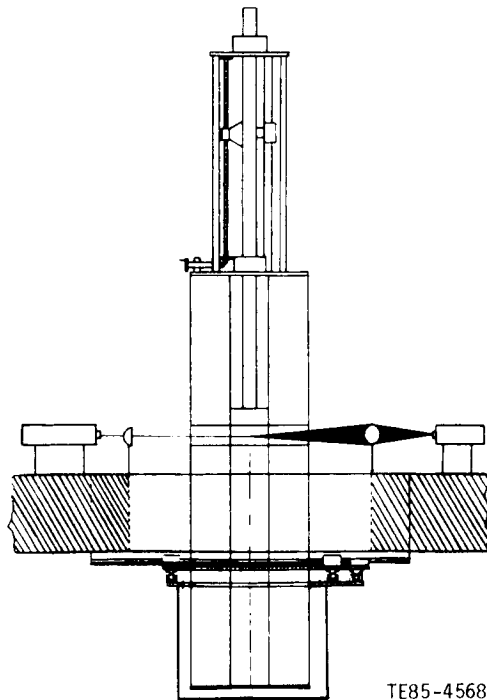injector with 60 deg swirler).

105

DPL2SG
VELOCITY VECTORS
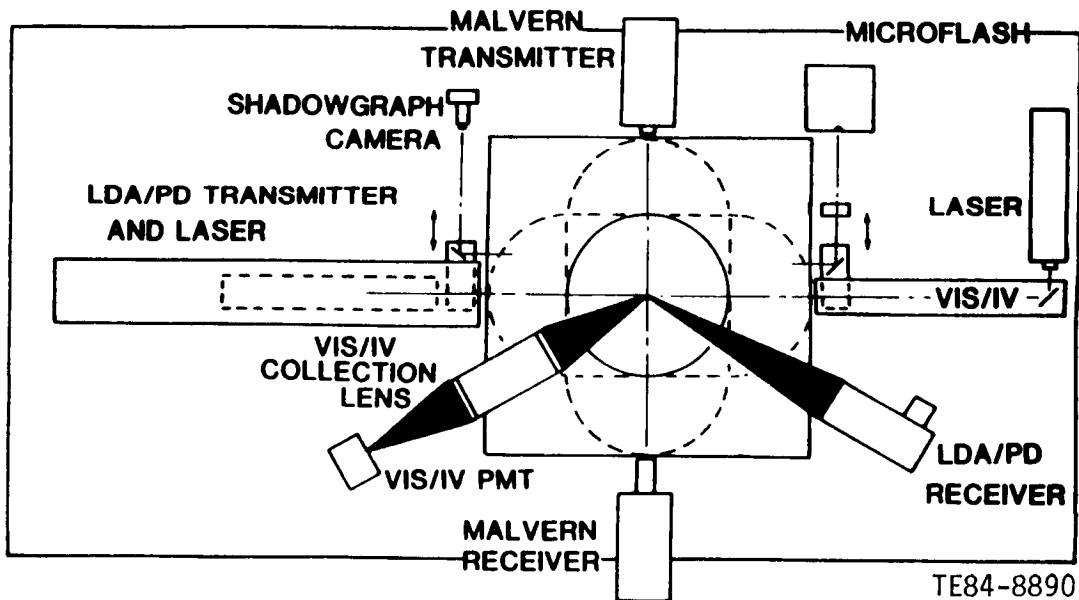

DPL2SG
FLOW STREAMLINES

DPL2SG
PARTICLE TRAJECTORIES
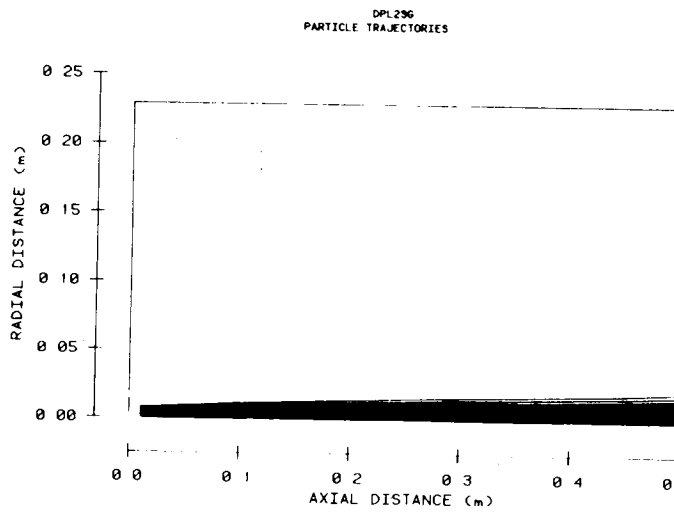
TE85-2826

Figure 12.   Methanol spray dispersion at unconfined conditions
(fuel nozzle surrounded by low velocity stream).

106

TE85-4568

MALVERN
TRANSMITTER

MICROFLASH

SHADOWGRAPH
CAMERA

LDA/PD TRANSMITTER
AND LASER

LASER

VIS/IV

VIS/IV
COLLECTION
LENS

VIS/IV PMT

LDA/PD
RECEIVER

MALVERN
RECEIVER

TE84-8890

Figure 13.   Flow facility and optical arrangement.
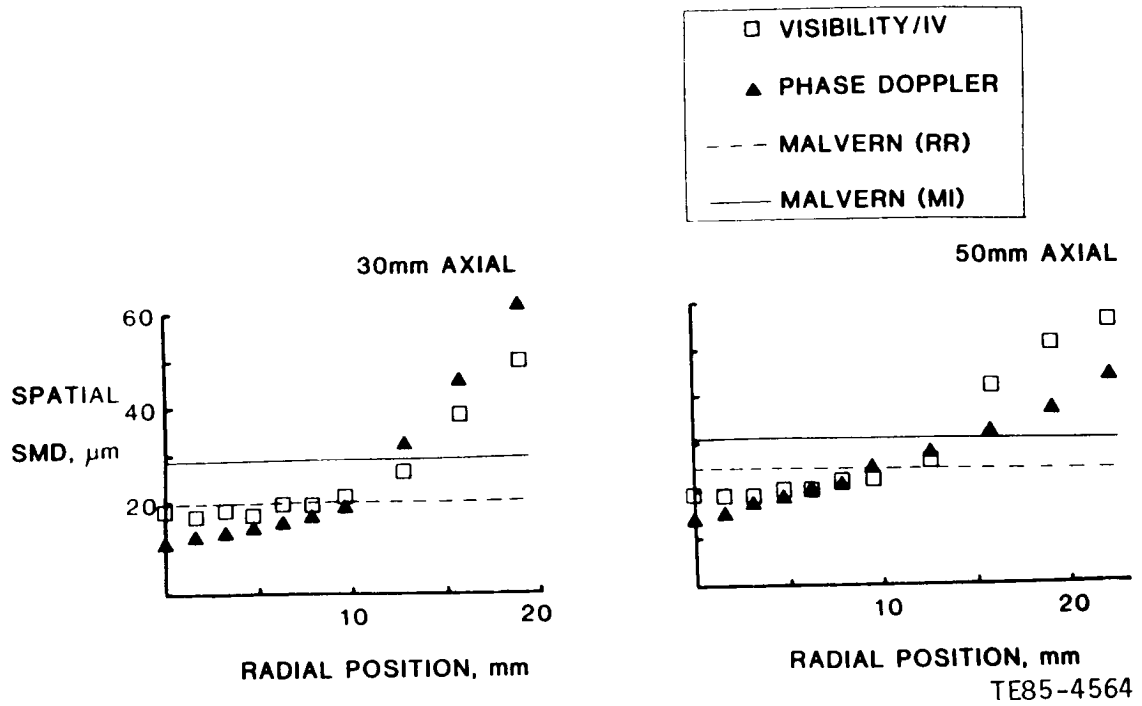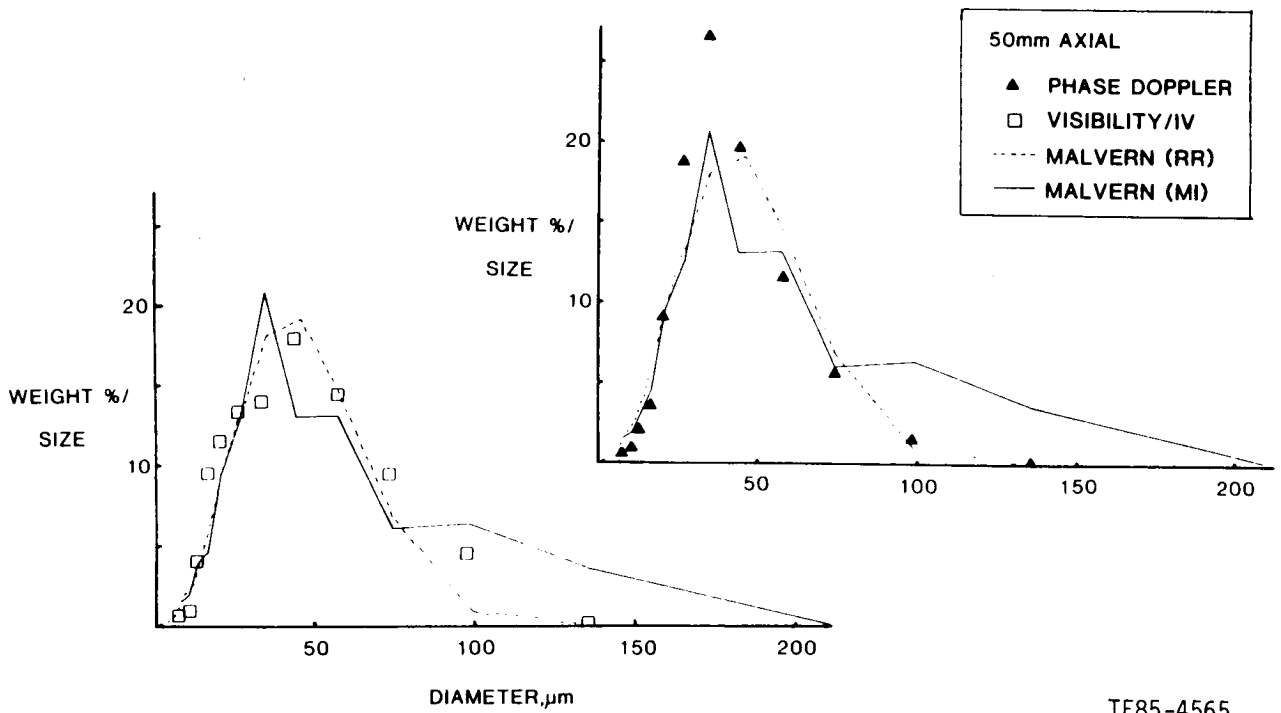
Figure 14.   Radial profile of spatial SMD.

Figure 15.   Mass distribution comparison.

108